Improved Description of Chemical Barriers with Generalized Gradient Approximations (GGAs) and Meta-GGAs

M. Grüning, O. V. Gritsenko, and E. J. Baerends*

Section Theoretical Chemistry, Vrije Universiteit, De Boelelaan 1083, 1081 HV Amsterdam, The Netherlands

Received: November 5, 2003; In Final Form: March 9, 2004

The performance of exchange and correlation (xc) functionals of the generalized gradient approximation (GGA) type and of the meta-GGA type in the calculation of chemical reactions is related to topological features of the electron density which, in turn, are connected to the orbital structure of chemical bonds within the Kohn−Sham (KS) theory. Seventeen GGA and meta-GGA xc functionals are assessed for 15 hydrogen abstraction reactions and 3 symmetrical S_N2 reactions. Systems that are problematic for standard GGAs characteristically have enhanced values of the dimensionless gradient argument s_σ^2 with local maxima in the bonding region. The origin of this topological feature is the occupation of valence KS orbitals with an antibonding or essentially nonbonding character. The local enhancement of s_σ^2 yields too negative exchange−correlation energies with standard GGAs for the transition state of the S_N2 reaction, which leads to the reduced calculated reaction barriers. The unwarranted localization of the effective xc hole of the standard GGAs, i.e., the nondynamical correlation that is built into them but is spurious in this case, wields its effect by their s_σ^2 dependence. Barriers are improved for xc functionals with the exchange functional OPTX as x component, which has a modified dependence on s_σ^2. Standard GGAs also underestimate the barriers for the hydrogen abstraction reactions. In this case the barriers are improved by correlation functionals, such as the Laplacian-dependent (LAP3) functional, which has a modified dependence on the Coulomb correlation of the opposite- and like-spin electrons. The best overall performance is established for the combination OLAP3 of OPTX and LAP3.

I. Introduction

It is common practice in density functional theory (DFT) to derive the functional form of its exchange−correlation (xc) functionals from the homogeneous/inhomogeneous electron gas model or from prototype atomic systems. Their performance for molecular systems and chemical reactions then becomes, to some extent, a matter of accident. In this typical situation, it is essential to understand the factors which determine the quality of molecular DFT calculations and to identify cases which are problematic for DFT functionals. Such cases have been identified in the literature,[3−18] and in ref 19, a qualitative rule has been put forward to predict success or failure of standard generalized gradient approximations (GGAs).[20−23] Problematic molecular systems and transition states (TSs) of chemical reactions with a particular chemical bond have been identified in ref 19 by a noninteger ratio n/m of the number, n, of electrons involved in the bond to the number, m, of relevant fragment orbitals.

The prototype cases discussed in the literature are radical abstraction reactions

$$X^\bullet + R{-}Y \rightarrow X{-}R + Y^\bullet \qquad (1.1)$$

and the S_N2 reaction

$$X^- + ZY \rightarrow XZ + Y^- \qquad (1.2)$$

Standard GGA methods tend to underestimate barriers of both reactions (1.1) and (1.2) due to the overestimated stability of their TSs (refs 7, 9, 11, 16, and 17 and Tables 1−8 below). Note, however, that according to the rule of ref 19, the cases of (1.1) and (1.2) belong to different types. In the radical abstraction reaction (1.1), a three-center ($m = 3$) three-electron ($n = 3$) bond is formed in its open-shell TS, so that with the integer ratio $n/m = 1$ the TS belongs to "normal" systems. Improved description of such systems does not require alteration of the dominant GGA exchange energy functional $E_x^{GGA}[\rho]$. Instead, it was recommended in ref 3 to modify the relatively small GGA correlation energy functional $E_c^{GGA}[\rho]$, more precisely, the dependence of E_c^{GGA} on the local spin polarization $\zeta(\mathbf{r}) = [\rho^\alpha(\mathbf{r}) - \rho^\beta(\mathbf{r})]/\rho(\mathbf{r})$. On the other hand, in the closed-shell TS of the S_N2 reaction (1.2), a three-center ($m = 3$) four-electron ($n = 4$) bond is formed. With the noninteger ratio $n/m = 4/3$ this TS belongs to truly "problematic" systems, the proper description of which requires improvement of E_x^{GGA}.

In this paper, a further step is made, and the performance of xc functionals is related to topological features of the molecular electron density which, in turn, are connected with the orbital structure of chemical bonds within the Kohn−Sham (KS) theory. Seventeen xc functionals are assessed for 15 hydrogen abstraction reactions and 3 symmetrical S_N2 reactions. One group of functionals considered are the standard GGAs and their recent modifications, in which the local density approximations (LDAs) for exchange and correlation are corrected with functions of the dimensionless argument s_σ containing the spin-density gradient $\nabla\rho_\sigma$

$$s_\sigma(\mathbf{r}) = \frac{1}{2(6\pi^2)^{1/3}} \frac{|\nabla\rho_\sigma(\mathbf{r})|}{\rho_\sigma^{4/3}(\mathbf{r})} \qquad (1.3)$$

* To whom correspondence should be addressed. E-mail: baerends@chem.vu.nl.

10.1021/jp031227u CCC: $27.50
Published on Web 04/20/2004

Another group of functionals are meta-GGAs, which depend also on the Kohn−Sham (KS) kinetic energy spin-density $\tau_\sigma^s(\mathbf{r})$ in its gradient (rather than Laplacian) form:

$$\tau_\sigma^s(\mathbf{r}) = \frac{1}{2}\sum_i^{N_\sigma} |\nabla\phi_{i\sigma}(\mathbf{r})|^2 \qquad (1.4)$$

and/or on the Laplacian of the spin-density $\nabla^2\rho_\sigma$.

In Section II of the paper, the behavior of the basic GGA argument $s_\sigma^2(z)$ along the bond axis z is analyzed for N_2, a prototype molecule with covalent bonds, He_2^+, a prototype problematic molecule with a two-center three-electron bond ($n/m = 3/2$), the TSs H···Cl···H of the hydrogen exchange and H··H··H of the hydrogen abstraction reactions, and the TS $[F\cdots CH_3\cdots F]^-$ of the S_N2 reaction. The topology of the density in the problematic cases is characterized by a local maximum (or maxima) of s_σ^2 in the bonding region. The orbital origin of this topological feature is established: the occupation of KS orbitals with an antibonding or essentially nonbonding character. This allows us to rationalize the failure in the problematic cases of the standard GGAs, for which terms with s_σ^2 dominate the gradient correction for the exchange functional. It also provides an explanation of the improved performance for the S_N2 reactions (described in Section V) of modified GGA exchange functionals, for which terms with the fourth power s_σ^4 of the argument s_σ actually dominate the gradient correction. In Section III, the behavior along the bond axis of the meta-GGA correction factor f_σ, which is a function of $\tau_\sigma^s(\mathbf{r})$, is analyzed for the abovementioned prototype systems. This analysis rationalizes the improved performance of meta-GGAs for the S_N2 reactions. In Section IV, the results of calculations of the symmetrical S_N2 reactions are presented. In agreement with the analysis of ref 19, alteration of the exchange functionals produces the most substantial improvement of the calculated central and overall reaction barriers. In Section V, the results of the GGA and meta-GGA calculations of the hydrogen abstraction reactions are presented. In this case, as expected from ref 19, modified correlation energy functionals produce substantial improvement of the calculated forward and reverse reaction barriers. An original combination, OLAP3, of the modified GGA exchange OPTX functional[1] and the τ_σ^s-dependent correlation functional LAP3[2] shows the best overall performance for both hydrogen abstraction and symmetrical S_N2 reactions. The chemically important prototype reaction of hydrogen abstraction from the water molecule

$$H_2O + OH^\bullet \rightarrow OH^\bullet + H_2O \qquad (1.5)$$

is a somewhat special case. OLAP3 gives a barrier of 3.69 kcal/mol, which deviates by only 0.51 kcal/mol from the experimental estimate of 4.2 kcal/mol of the activation energy, although it differs considerably from the best theoretical estimate of 10.1 kcal/mol from QCISD(T) calculations. In Section VI, the conclusions are drawn.

II. Behavior of s_σ^2 and Its Relation to the Orbital Nature of the Chemical Bond

To understand the abovementioned, uneven performance of the GGA exchange functionals for various types of systems, we analyze the behavior of their basic argument s_σ^2 for prototype systems. This approach is justified since standard GGA exchange functionals can be considered as extensions of the gradient expansion approximation (GEA),[24] with the latter being the LDA exchange functional corrected just with $-\beta s_\sigma^2$ (β is a positive coefficient). In our paper, standard GGA exchange functionals are represented with those of Becke (B88),[23] Perdew and Wang (PW91),[21,25,26] and Perdew, Burke, and Ernzerhof (PBE).[27]

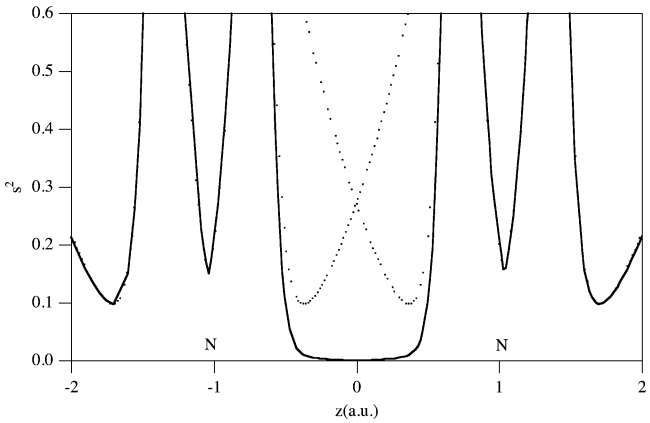

Figure 1. s^2 (1.3) is plotted along the bond axis of the N_2 molecule (line). s^2 (1.3) for the atoms is plotted at the atomic positions (dots).

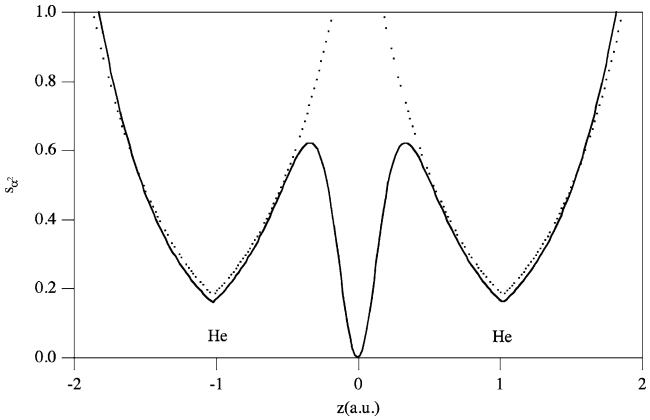

Figure 2. s_α^2 (1.3) is plotted along the bond axis of the He_2^+ cation dimer (line). s^2 (1.3) for the atoms is plotted at the atomic positions (dots).

A typical behavior of s_σ^2 for a strong covalent bond is presented in Figure 1, where it is plotted along the bond axis z of the N_2 molecule. Distinguishing features of the plot are the divergence of $s_\sigma^2(z)$ at the asymptotics $|z| \rightarrow \infty$ and in the bulk region, strong local maxima in the atomic regions, and nearly complete vanishing of $s_\sigma^2(z)$ in the bonding region. The strong peaks in the atomic regions within ca. ± 0.5 bohr of the nuclear postions are clearly atomic in origin, as is obvious from the plots of the atomic $s_\sigma^2(z)$ (dotted curves). As was discussed in ref 28, the change of s_σ^2 in the bond region ($|z| \leq 0.5$), from very large values in the atoms to practically zero in the molecule, leads the s_σ^2-dependent GGAs to correct the overbinding produced with LDA for covalent bonds. As was argued in ref 29 for the LDA and in refs 3, 19, and 30 for the GGA, these exchange functionals with their localized model exchange holes represent effectively not only exchange but also nondynamical Coulomb correlation (or at least left−right correlation in two-center bonds). According to ref 30, the GGA correction of the exchange which is affected through its s_σ^2 dependence makes the GGA "exchange" functionals represent exchange plus nondynamical correlation very accurately.

A typical behavior of s_α^2 (α is the major spin) for a problematic molecule is presented in Figure 2, where it is plotted for He_2^+. In this case, unlike for N_2, $s_\alpha^2(z)$ is clearly nonzero (positive) in the bonding region and, before going to the required zero value due to the zero density gradient at the bond midpoint,

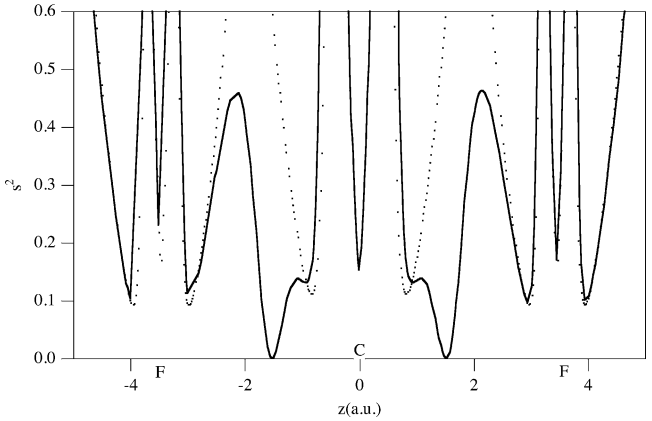

Figure 3. s^2 (1.3) is plotted along the bond axis of the TS of the S_N2 reaction $[F\cdots CH_3\cdots F]^-$ (line). s^2 (1.3) for the atoms is plotted at the atomic positions (dots).

s_α^2 increases with increasing distance from the nearest He nucleus, so that it displays two symmetrical local maxima of heights ≈ 0.6 at $z \approx \pm 0.25$ au. Note that the atomic s_α^2 do not exhibit the near-nuclear maxima that were observed for the N atom, but are monotonically increasing from the nucleus outward. This is a consequence of the single 1s shell of He. To understand the topological feature of the density that is represented with the s_α^2 behavior in the bond region, we recall that the two-center three-electron bond $[He_A-He_B]^+$ is represented, essentially, by double occupancy of the $\phi_g = (a + b)/\sqrt{2+2S}$ (S is the overlap integral between a and b) bonding KS molecular orbital (MO) between 1s atomic orbitals (AOs) a and b on He_A and He_B and single occupancy of the antibonding combination $\phi_u = (a - b)/\sqrt{2-2S}$. In this case, a straightforward calculation of the corresponding $s_\alpha^2(z)$ for a point z on the axis between He_A and He_B shows that it is proportional to the following combination of the orbital densities $\phi_{g\alpha}^2$ and $\phi_{u\alpha}^2$

$$s_\alpha^2(z) \cong \frac{1}{[\phi_{g\alpha}^{4/3}(z)]} \frac{x(z)}{[x(z)+1]^{8/3}} \qquad (2.1)$$

where $x = \phi_{u\alpha}^2/\phi_{g\alpha}^2$ is the ratio of these densities and we have used $\nabla\phi_g(z) = -\sqrt{[(2-2S)/(2+2S)]}\phi_u(z)$. The second, x-dependent fraction of (2.1) displays two symmetrical local maxima in the bonding region at $x = 3/5$. Note that, in reality, x decreases from its infinite (due to the more diffuse nature of $\phi_{u\alpha}$, which is not reflected in our simplistic model leading to eq 2.1) value at the asymptotics $z \to \infty$ to $x = 0$ at the bond midpoint, where $\phi_{u\alpha}$ has a node, so that $x = 3/5$ is well within the bonding region. The first fraction of (2.1) which increases when going from the nuclei to the bond midpoint should then shift the local maxima of $s_\alpha^2(z)$ further toward the bond midpoint. Thus, the expression (2.1) explains the appearance of the local maxima of $s_\alpha^2(z)$ in the bonding region of He_2^+ as the result of occupation of the antibonding orbital $\phi_{u\alpha}$. Note that this feature is related to the type of bond, in contrast to the large peaks in Figure 1 that have an atomic origin.

To see whether this topological feature appears also for the considered problematic case of the TS of the S_N2 reaction, we plot in Figure 3 $s_\sigma^2(z)$ for the TS $[F\cdots CH_3\cdots F]^-$. Indeed, besides pronounced atomic shell structure for the two terminal F atoms and the central C atom, Figure 3 displays also distinct local maxima of height ≈ 0.45 at $z \approx \pm 2.1$ au in the regions between the F nuclei and the nodes of s_σ^2. They indicate essentially nonbonding character of the orbitals ϕ_0 and ϕ_+ participating in the three-center four-electron σ-interaction F···C···F (see Figure 4). The highest occupied molecular orbital (HOMO) ϕ_0 is, predominantly, the in-phase combination of p_σ orbitals of the F atoms, $\phi_0 \approx c_0[\sigma(F_A) + \sigma(F_B)]$, which is only very weakly σ bonding within the fragment $[F_A\cdots F_B]^-$, due to the large distance. The lower lying occupied MO ϕ_+ is actually the out-of-phase combination of σ orbitals of $[F_A\cdots F_B]^-$, stabilized by admixture of the p_σ orbital of the C atom, $\phi_+ \approx c_{1+}[\sigma(F_A) - \sigma(F_B)] - c_{2+}\, p_z(C)$. The doubly occupied ϕ_+ and ϕ_0 together are, except for the p_z(C) admixture, equivalent to two nonbonding atomic p_σ lone pairs. This nonbonding atomic orbital character is reflected in a steady increase of s_σ^2 with decreasing $|z|$ in the bonding regions, i.e., in the intervals $3 > |z| > 2.1$ au beyond the inner shell structure of the F atoms. This increase is similar to the increase of s_σ^2 in the regions of the nonbonding lone-pair orbitals on the outer sides of the F atoms (see Figure 3). Due to the bonding contribution of the p_z orbital of the C atom to the MO ϕ_+, the bonding regions between the nodes of s_σ^2 and the inner shell structure of the C atom are characterized with relatively low values of s_σ^2, attributed to covalent bonding. Combination of the discussed features produces for the TS $[F\cdots CH_3\cdots F]^-$ the observed double local maxima of $s_\sigma^2(z)$ around its zero points, with different heights at the F and C sides.

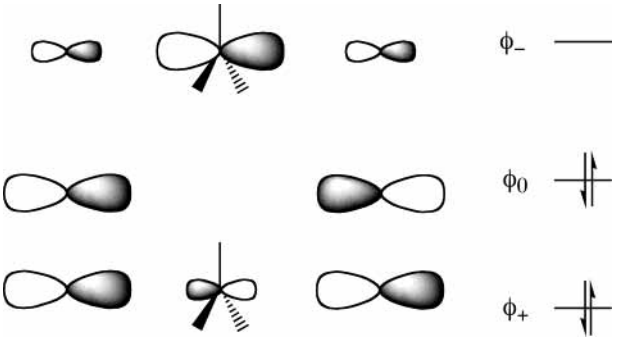

Figure 4. Orbitals participating in the four-electron three-orbital interaction of the TS of the S_N2 reaction $[F\cdots CH_3\cdots F]^-$.

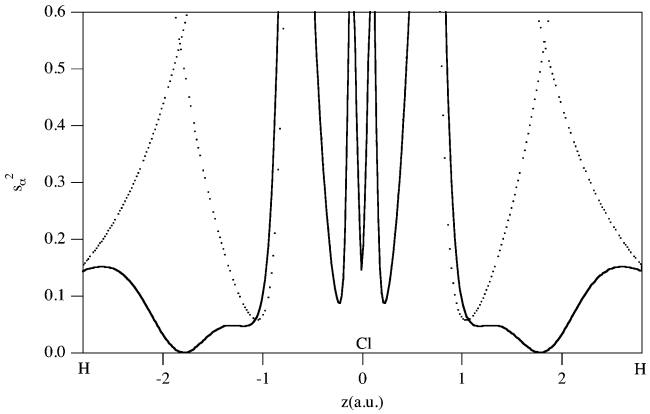

Figure 5. s_α^2 (1.3) is plotted along the bond axis of the prototype hydrogen exchange TS $[H\cdots Cl\cdots H]$ (line). s^2 (1.3) for the atoms is plotted at the atomic positions (dots).

In Figure 5, $s_\alpha^2(z)$ is plotted for the hydrogen exchange TS $[H\cdots Cl\cdots H]$ which, according to the rule of ref 19, is another example of a normal system besides the N_2 molecule considered in Figure 1. Note that the Cl atomic structure of $s_\alpha^2(z)$ consists of four peaks: a K shell doublet at $z = \pm 0.1$ bohr, and an L shell doublet at $0.25 \le |z| \le 1.1$ bohr. Again in agreement with this rule, the behavior of s_α^2 in the region of the H···Cl bonds beyond the Cl atomic shell structure is closer to the vanishing pattern of s_σ^2 in the N_2 bonding region (see Figure 1) than the behavior of s_σ^2 in the corresponding regions of He_2^+

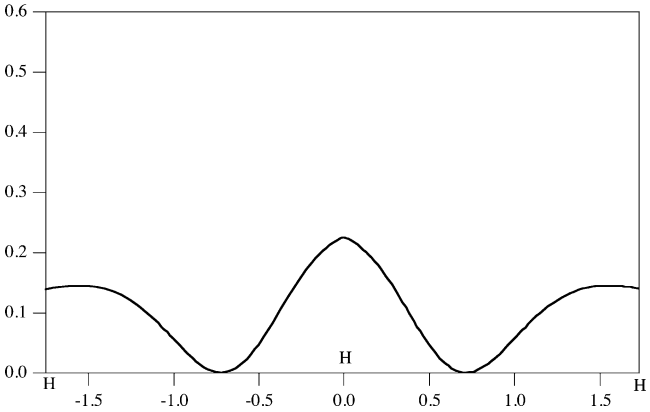

Figure 6. s_α^2 (1.3) is plotted along the bond axis of the prototype hydrogen abstraction TS [H···H···H].

(Figure 2) and $[F\cdots CH_3\cdots F]^-$ (Figure 3). Indeed, as one can see from Figure 5, in the bonding region between the pronounced atomic shell structure of the Cl atom and the characteristic "plateau" around the H nucleus for the hydride H atom, the argument s_α^2 is rather flat. It does not display pronounced maxima, and its values in these regions are much smaller compared to those in the bonding regions of the problematic systems considered above. Figure 6 presents $s_\alpha^2(z)$ for the prototype hydrogen abstraction TS [H···H···H]. Again, besides the atomic peak around the central H atom and the abovementioned plateaus around the terminal H atoms, there are no local maxima in the bonding region, where $s_\alpha^2(z)$ decreases monotonically toward its bond-midpoint nodes (see Figure 6).

A characteristic topological feature of the density of problematic systems that emerges from this comparative analysis is the enhanced values of s_σ^2 with local maxima in the bonding regions. The origin of this enhancement is the occupation of valence orbitals with an antibonding or essentially nonbonding character. In reality, as was argued in refs 18 and 19, occupation of antibonding orbitals hampers nondynamical correlation. However, the accompanying s_σ^2 enhancement leads to more strongly negative energies from the GGA exchange functionals. The s_σ^2 enhancement can be considered to build in spurious correlation through the increased contributions of GGA gradient corrections from the bonding regions. This causes the abovementioned overestimation by standard GGAs of the stability of problematic systems. More enhanced values and higher maxima of s_σ^2 in the bonding region of He_2^+ compared to those for $[F\cdots CH_3\cdots F]^-$ (compare Figures 2 and 3) correlate with larger GGA errors for the former system.[5,18]

The analysis performed in this section helps in understanding the possibility of the improvement for problematic cases offered by the recent modified GGA exchange functionals, namely, the functional of the optimal exchange method (OPTX) of Cohen and Handy[1] and that of the method of Hamprecht, Cohen, Tozer, and Handy (HCTH).[31] Unlike standard GGAs, both OPTX and HCTH have as their zero-gradient limit the Xα exchange functional, in which the parameter α is enhanced by ca. 1.05 compared to its standard LDA value. Another difference is that both functionals effectively have the fourth power s_σ^4 as the leading power of their gradient corrections in the bulk region. Since the values of s_σ in the bonding regions are less than 1 for all prototype systems considered (see Figures 1−6), the contributions from the gradient corrections to the bond energy are reduced in OPTX and HCTH, which might substantially correct the relative over-stability of standard GGAs for problematic systems.

In Sections IV and V, the performance of GGAs will be assessed for the S_N2 and hydrogen abstraction reactions. In this assessment, the abovementioned exchange functional B88 is taken in standard combinations: BLYP and BP with the GGA correlation energy functionals of Lee, Yang, and Parr (LYP)[22] and Perdew (P86).[20] Also, the combination, OLYP, of the exchange functional OPTX and the correlation functional LYP is considered. GGA exchange functionals PW91, PBE, and HCTH mentioned in this section are taken with "their own" correlation functionals, so that their abbreviations in the subsequent tables are extended to the corresponding exchange−correlation (xc) combinations.

An alternative way of improvement is offered by meta-GGAs with their dependence on τ_σ^s of (1.4). This will be analyzed in the next section.

III. Behavior of τ_σ^s and the Performance of Meta-GGAs

The KS kinetic energy density τ_σ^s (1.4) is usually employed in meta-GGAs as the denominator of the ratio t_σ,

$$t_\sigma(\mathbf{r}) = \frac{\tau_\sigma^{\mathrm{LSDA}}(\mathbf{r})}{\tau_\sigma^s(\mathbf{r})} \tag{3.1}$$

where $\tau_\sigma^{\mathrm{LSDA}}$

$$\tau_\sigma^{\mathrm{LSDA}}(\mathbf{r}) = \frac{3}{10}(6\pi^2)^{2/3}\rho_\sigma^{5/3}(\mathbf{r}) \tag{3.2}$$

is the local spin-density approximation (LSDA) for the kinetic energy density. The basic point of our further analysis is that the meta-GGA argument t_σ is actually closely related to the GGA argument s_σ. Indeed, the KS τ_σ^s of (1.4) can be expressed as the sum

$$\tau_\sigma^s(\mathbf{r}) = \tau_\sigma^{\mathrm{W}}(\mathbf{r}) + \tau_\sigma^{\mathrm{P}}(\mathbf{r}) \tag{3.3}$$

of the von Weiszäcker τ_σ^{W}

$$\tau_\sigma^{\mathrm{W}}(\mathbf{r}) = \frac{1}{8}\frac{|\nabla\rho_\sigma(\mathbf{r})|^2}{\rho_\sigma(\mathbf{r})} \tag{3.4}$$

and Pauli τ_σ^{P}

$$\tau_\sigma^{\mathrm{P}}(\mathbf{r}) = \frac{\rho_\sigma(\mathbf{r})}{2}\sum_i^{N_\sigma}\left|\nabla\frac{\phi_{i\sigma}(\mathbf{r})}{\rho_\sigma^{1/2}(\mathbf{r})}\right|^2 \tag{3.5}$$

terms. In the region of localization of a certain occupied KS orbital $\phi_{i\sigma}$, where it dominates ρ_σ, the Pauli term (3.5) vanishes, and τ_σ^s turns to (3.4)

$$\tau_\sigma^s(\mathbf{r}) \approx \frac{1}{8}\frac{|\nabla\rho_\sigma(\mathbf{r})|^2}{\rho_\sigma(\mathbf{r})} \tag{3.6}$$

With (3.6), the meta-GGA argument t_σ becomes just proportional to the inverse of s_σ^2:

$$t_\sigma(\mathbf{r}) \approx \left[\frac{3}{10}(6\pi^2)^{2/3}\rho_\sigma^{5/3}(\mathbf{r})\right]\left[\frac{1}{8}\frac{|\nabla\rho_\sigma(\mathbf{r})|^2}{\rho_\sigma(\mathbf{r})}\right]^{-1} = \frac{3}{5s_\sigma^2(\mathbf{r})} \tag{3.7}$$

When other orbitals $\phi_{j\neq i\sigma}(\mathbf{r})$ have appreciable local contributions to $\rho_\sigma(\mathbf{r})$, the argument t_σ of (3.1) could be substantially smaller than its estimate $0.6s_\sigma^{-2}$ from (3.7). Still, the expression

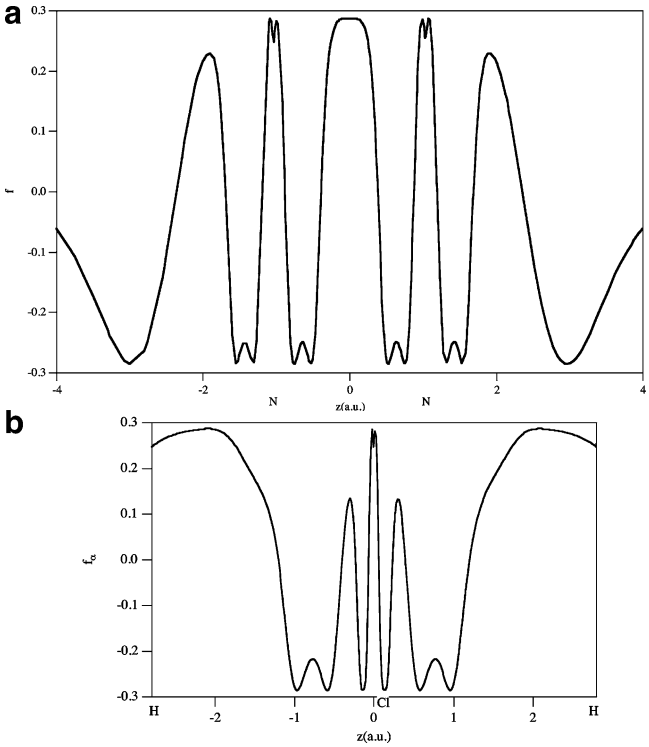

Figure 7. (a) f (3.9) is plotted along the bond axis of the N_2 molecule. (b) f_α (3.9) is plotted along the bond axis of the prototype hydrogen exchange TS [H···Cl···H].

(3.7) provides a rough idea of the relation between t_σ and s_σ^2 and of how t_σ could be employed in meta-GGAs.

The use of t_σ in meta-GGAs can be illustrated with the t_σ-dependent function $f_\sigma(t_\sigma)$, which is employed in the meta-GGA exchange functional of Becke (B00)[32] as a correction factor:

$$E_{x\sigma}^{\mathrm{B00}} = \int \{1 + a f_\sigma[t_\sigma(\mathbf{r})]\} e_{x\sigma}^{\mathrm{BR89}}(\mathbf{r})\, \mathrm{d}\mathbf{r} \qquad (3.8)$$

In (3.8) $e_{x\sigma}^{\mathrm{BR89}}$ is the energy density of the exchange functional of Becke and Roussel (BR89) obtained from a model-localized Fermi hole[33] and a is an empirical parameter, which in B00 is 0.14. The correction factor f_σ is defined as follows:

$$f_\sigma = w_\sigma - 2{w_\sigma}^3 + {w_\sigma}^5 \qquad (3.9)$$

where the auxiliary argument w_σ is the following function of t_σ:

$$w_\sigma(\mathbf{r}) = \frac{t_\sigma(\mathbf{r}) - 1}{t_\sigma(\mathbf{r}) + 1} \qquad (3.10)$$

By the construction (3.8), positive values of $f_\sigma(\mathbf{r})$ make the energy $E_{x\sigma}^{\mathrm{B00}}$ more strongly negative, while negative $f_\sigma(\mathbf{r})$ makes $E_{x\sigma}^{\mathrm{B00}}$ less negative.

In Figures 7 and 8, the correction factor f_σ is plotted for the prototype systems considered in the previous section. By its design, the function $f_\sigma(z)$ oscillates in the molecular regions, while it vanishes at the long-range asymptotics. Such an oscillatory behavior is required in order to maintain the overall energy balance achieved with the uncorrected functional BR89. However, the oscillation patterns are different for normal systems N_2 and [H···Cl···H], on one hand, and for problematic systems He_2^+ and $[F{\cdots}CH_3{\cdots}F]^-$, on the other hand. Indeed, while $f_\sigma(z)$ is generally positive in the bonding regions of normal systems (see Figure 7a and b), it is negative in the bonding

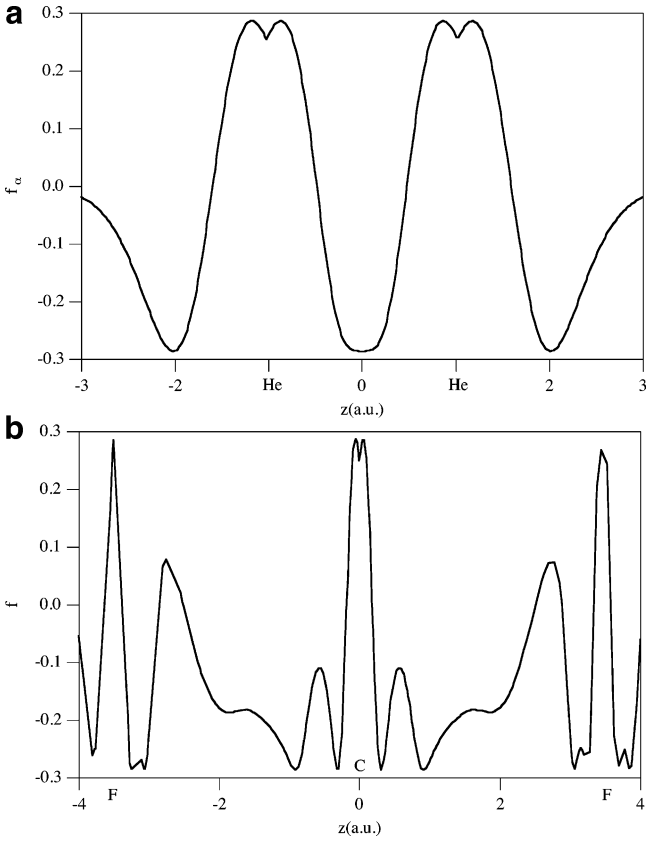

Figure 8. (a) f (3.9) is plotted along the bond axis of the He_2^+cation dimer. (b) f_α (3.9) is plotted along the bond axis of the TS of the S_N2 reaction $[F{\cdots}CH_3{\cdots}F]^-$.

regions of problematic systems (see Figure 8a and b). With this, the correction factor f_σ should reduce the energy contributions from the bonding regions, which are too strongly negative for problematic systems with the uncorrected functionals. As follows from the construction (3.8)−(3.10), from the approximate relation (3.7) between t_σ and s_σ, and from the analysis of s_σ presented in the previous section, the abovementioned characteristic pattern of f_σ with negative values in the bonding regions can be traced to the occupation of orbitals with an antibonding character in the problematic cases.

In the next sections, the performance of meta-GGAs will be assessed for the S_N2 and hydrogen abstraction reactions. In this assessment, the abovementioned exchange functionals B00 and BR89 are taken in combinations B00c and BR89c with the correlation functional of Becke (Bc88).[34,35] Among other meta-GGAs considered are the xc functionals of Van Voorhis and Scuseria (VS98)[36] and of Perdew, Kurt, Zupan, and Blaha (PKZB).[37] The exchange part of PKZB is also combined with the meta-GGA correlation functional of Krieger, Chen, Iafrate, and Savin (KCIS).[38] Other meta-GGA correlation functionals considered are LAP3 of Proynov, Sirois, and Salahub[2] and its modified version τ1 of Proynov, Chermette, and Salahub.[39] They are taken in combinations Bmτ1 and BLAP3 with the (modified) exchange functional B88. LAP3 is also combined in this paper with the abovementioned modfied GGA exchange functional OPTX (with leading s_σ^4 dependence, see previous section) to form the xc combination OLAP3.

IV. Assessment of GGAs and Meta-GGAs for S_N2 Reactions

The prototype S_N2 reaction considered in this paper is the following symmetrical substitution of the halide anion X^-:

$$X^- + CH_3X \rightarrow XCH_3 + X^- \qquad (4.1)$$

where X = F, Cl, or Br. The reaction goes through the formation of an unsymmetrical ion−dipole intermediate complex (IC) $X^-\cdots CH_3X$ and symmetrical TS $[X\cdots CH_3\cdots X]^-$. The special case for which X = F was considered in the previous sections. These intermediates determine the key parameters of the reaction (4.1): the complexation energy E_{cmpx}, which is the energy difference between IC and free reagents, the central barrier E_{centr}, which is the energy difference between TS and IC, and the overall barrier E_{ovr}, the energy difference between TS and free reagents. The intermediates IC and TS, the barriers, and E_{cmpx} are schematically shown in Figure 9.

All GGA and meta-GGA calculations have been performed with the Amsterdam Density Functional (ADF) program.[40−42] Geometries for reagents, IC, and TS were taken from ref 43. All self-consistent calculations have been performed with the BLYP xc potential, so that, for other functionals, the energies E_{cmpx}, E_{centr}, and E_{ovr} have been calculated in the post-BLYP manner. The error of not calculating the energy self-consistently can be estimated to be of the order of a few tenths kilocalories per mole. The reference data for these energies are the results of ab initio coupled-cluster CCSD(T) calculations for X = F[44] and experimental data for X = Cl and Br.[45−49] In Table 1 we also report alternative calculated[43] and experimental values[47,50,51] to give our chosen reference values a sense of proportion. For X = F, the values calculated with the G2(+)[43] method are close to or within the error bars of the results from the CCSD(T) calculations[44] (zero point vibrational energy and higher corrections are also within these error bars). For X = Br, the G2-(+)[43] (with the use of effective core potentials for the core electrons) calculated energies are again close to the experimental values. In the case where X = Cl, larger discrepancies are found between the two experimental E_{cmpx},[45,47] while the G2(+)[43] calculated value is between them.

The calculations have been carried out in the triple-ζ basis + polarization functions (TZ2P) of Slater-type orbitals (STOs). For X = F and for X = Cl, a larger basis set with very diffuse basis functions is needed for the convergence of the bond energy of the anion.[52] In our calculations the available standard ADF quadruple-ζ (for valence orbitals) and double-ζ (for core orbitals) even-tempered basis set augmented with three polarization functions (ETQZ3P) and the similar basis ETQZ + 5P (with five polarization functions and, in addition, one set of tight and one set of diffuse s and p STOs) have been used respectively for Cl and F. We estimate the remaining basis set error on the reaction barriers of the order of 0.1−0.2 kcal/mol. Further, neither zero point vibrational energy nor thermal corrections are applied when our calculated data are compared with the experimental values. This also introduces an error of a few tenths kilocalories per mole.

Absolute values of the calculated energies E_{cmpx}, E_{centr}, and E_{ovr} for X = F, Cl, and Br are compared with the reference data in Table 1. In Table 2, the corresponding errors of LDA, GGAs, and meta-GGAs are shown. Table 3 presents the mean average error for the three reactions considered. One can see from these tables the important difference between LDA and standard GGAs, on one hand, and modified GGAs and meta-GGAs, on the other hand. LDA reproduces satisfactorily the reference complexation energies E_{cmpx}. More precisely, it slightly overestimates the relative stability of the IC with the average error $\Delta E_{cmpx}^{LDA} = -2.65$ kcal/mol (see Table 3). However, the abovementioned, typical LDA tendency to overbind is much more pronounced for the TS. According to the reference data,

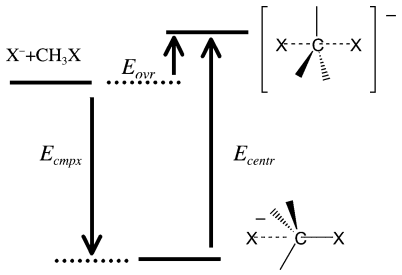

Figure 9. Schematic representation of the intermediates IC and TS, the barriers, and E_{cmpx} for the S_N2 reaction (4.1).

the TS is slightly more stable than reagents for X = F, and it is slightly less stable for X = Cl and Br (see Table 1). Conversely, LDA greatly overestimates the stability of the TS, which leads to the large negative values of −8 to −10 kcal/mol of E_{ovr}^{LDA} and small positive values of 3.5−6.5 kcal/mol for the central barrier E_{centr}^{LDA}.

Standard GGAs reduce the already not very significant LDA error for the complexation energy. Actually, PW91 and PBE yield the best E_{cmpx} values among all functionals, with absolute average errors of only 0.8 and 0.9 kcal/mol, respectively. However, standard GGAs fail to reduce significantly the large LDA errors for the barriers. Indeed, the LDA average error of 9.72 kcal/mol for the overall barriers is reduced to 6.2−9.7 kcal/mol with BLYP, BP, PW91, and PBE, and only revPBE reduces it to somewhat smaller 4.56 kcal/mol. Moreover, standard GGAs fail to reduce appreciably the LDA average error of 7.34 kcal/mol for the central barriers; in particular, the BLYP error of 7.52 kcal/mol is even slightly larger than that of the LDA (see Table 3). Notice that, while our results for the complexation energy for X = F substantially agree with the calculations at the BLYP level of approximation reported in ref 53, they differ noticeably for X = F and Cl from the results obtained in ref 54, where it was suggested that there is a sizable error of the LDA/GGAs. We attribute the differences with the calculations in ref 54 to the different basis sets used for the halides. (As we commented above, we use a very diffuse basis set for the halides, while in ref 54 a TZ2P basis set has been used. The TZ2P basis yields an energy for the F^- ion that is ca. 10 kcal/mol too high. Cf. also ref 52.)

An improved description of the barriers is achieved with the modified GGAs and meta-GGAs (see Tables 1−3). Since the functional B00 has been analyzed in the previous section as an example of the meta-GGA correction (in this particular case, the functional BR89 is corrected), it is instructive to compare the performance of the corresponding combinations B00c and BR89c. Due to the destabilizing effect of the correction factor f_σ of (3.8) and (3.9) on the TS, B00c yields improved higher central and overall barriers in all cases considered (see Tables 1 and 2). As a result, the average BR89c barrier errors $\Delta E_{ovr}^{BR89c} = 5.71$ kcal/mol and $\Delta E_{centr}^{BR89c} = 6.48$ kcal/mol are reduced in B00c to $\Delta E_{ovr}^{B00c} = 2.72$ kcal/mol and $\Delta E_{centr}^{B00c} = 4.15$ kcal/mol, respectively.

Combinations with the modified GGA exchange functional OPTX show the best performance. Indeed, the best overall barriers are produced with OLYP, with an average error of only 1.81 kcal/mol (see Table 3). It is clear that this improvement is solely due to OPTX, since the combination BLYP with the same standard correlation functional LYP produces much larger average error $\Delta E_{ovr}^{BLYP} = 6.74$ kcal/mol. Note that another modified GGA functional HCTH taken in combinations HCTH/93 and HCTH/407 produces nearly as good overall barriers as OLYP with the average error of 1.94 kcal/mol.

TABLE 1: Calculated Energies E_{cmpx}, E_{ovr}, and E_{centr} (kcal/mol) for the S_N2 Reactions (X = F, Cl, and Br)

	X = F			X = Cl			X = Br		
xc functional	E_{cmpx}	E_{ovr}	E_{centr}	E_{cmpx}	E_{ovr}	E_{centr}	E_{cmpx}	E_{ovr}	E_{centr}
LDA	−16.0	−9.5	6.4	−13.8	−8.4	5.4	−13.3	−9.7	3.5
PW91	−13.7	−6.7	7.1	−12.2	−6.7	5.6	−11.5	−7.8	3.8
BLYP	−12.6	−5.6	7.1	−10.9	−6.3	4.6	−10.1	−6.9	3.2
BP	−12.4	−5.2	7.1	−10.7	−5.4	5.3	−10.2	−6.6	3.6
PBE	−13.3	−5.9	7.4	−12.0	−6.1	6.0	−11.3	−7.1	4.1
revPBE	−11.3	−3.2	8.1	−10.5	−3.9	6.6	−9.8	−5.1	4.7
OLYP	−9.2	0.8	9.9	−9.1	−0.3	8.8	−8.0	−1.3	6.7
HCTH/93	−9.2	1.1	10.4	−8.8	−0.1	8.8	−8.0	−1.5	6.5
HCTH/407	−11.3	−0.5	10.8	−10.5	−0.7	9.8	−9.6	−2.5	7.1
KCIS	−11.2	−1.7	9.5	−9.7	−1.0	8.7	−9.3	−2.9	6.3
PKZB	−11.0	−1.5	9.5	−9.5	−1.1	8.4	−9.1	−2.9	6.2
VS98	−17.6	−5.8	11.7	−14.8	−5.3	9.6	−14.2	−7.1	7.1
Bmτ1	−11.8	−1.9	9.9	−10.8	−3.3	7.6	−11.0	−5.3	5.7
BLAP3	−11.7	−1.7	9.9	−10.6	−2.9	7.8	−10.8	−4.9	5.9
OLAP3	−8.2	4.6	12.8	−8.9	3.2	12.0	−8.8	0.6	9.4
B00c	−11.9	−1.5	10.4	−10.2	−1.9	8.3	−9.5	−3.3	6.2
BR89c	−12.8	−4.4	8.5	−10.5	−4.9	5.6	−10.3	−6.4	3.9
exp (ref values)				*−12.2± 2*[a]	*1 ± 1*[b]	*13.2 ± 2.2*[b]	*−9.2 ± 0.5*[c]	*1.3*[d]	*11.2*[e]
exp (other)				*−8.6 ± 0.2*[c]	*2.5*[f], *3.1*[g]				
calc (ref values)	*−13.7 ± 0.5*[h]	*−0.7*[h]	*13.0 ± 1.5*[h]						
calc (other)	*−13.5*[i]	*−1.9*[i]	*12.0*[i]	*−10.5*[i]	*2.8*[i]	*13.3*[i]	*−9.8*[i]	*1.4*[i]	*11.2*[i]

[a] Reference 46. [b] Reference 45. [c] Reference 47. [d] Reference 48. [e] Reference 49. [f] Reference 51. [g] Reference 50. [h] Reference 44. [i] Reference 43.

TABLE 2: Errors of the Calculated Energies ΔE_{cmpx}, ΔE_{ovr}, ΔE_{centr} (kcal/mol) with Respect to the Reference Data for the S_N2 Reactions (X = F, Cl, and Br)

	X = F			X = Cl			X = Br		
xc functional	ΔE_{cmpx}	ΔE_{ovr}	ΔE_{centr}	ΔE_{cmpx}	ΔE_{ovr}	ΔE_{centr}	ΔE_{cmpx}	ΔE_{ovr}	ΔE_{centr}
LDA	−2.3	−8.8	−6.6	−1.6	−9.4	−7.8	−4.1	−11.0	−7.7
PW91	−0.0	−6.0	−5.9	−0.0	−7.7	−7.7	−2.3	−9.1	−7.5
BLYP	1.1	−4.9	−6.0	1.4	−7.3	−8.6	−0.9	−8.2	−8.0
BP	1.4	−4.5	−5.9	1.5	−6.4	−7.9	−1.0	−7.9	−7.6
PBE	0.4	−5.2	−5.6	0.2	−7.1	−7.3	−2.1	−8.4	−7.1
revPBE	2.4	−2.5	−4.9	1.7	−4.9	−6.6	−0.6	−6.4	−6.5
OLYP	4.5	1.5	−3.1	3.1	−1.3	−4.3	1.2	−2.6	−4.5
HCTH/93	4.5	1.8	−2.6	3.4	−1.1	−4.4	1.2	−2.8	−4.7
HCTH/407	2.4	0.2	−2.2	1.7	−1.7	−3.4	−0.4	−3.8	−4.1
KCIS	2.5	−1.0	−3.5	2.5	−2.0	−4.5	−0.1	−4.2	−4.9
PKZB	2.7	−0.8	−3.5	2.7	−2.1	−4.8	0.1	−4.2	−5.0
VS98	−3.9	−5.1	−1.3	−2.6	−6.3	−3.6	−5.0	−8.4	−4.1
Bmτ1	1.9	−1.2	−3.1	1.4	−4.3	−5.7	−1.8	−6.6	−5.5
BLAP3	2.1	−1.0	−3.1	1.6	−3.9	−5.4	−1.6	−6.2	−5.3
OLAP3	5.5	5.3	−0.2	3.3	2.2	−1.2	0.4	−0.7	−1.8
B00c	1.8	−0.8	−2.6	2.0	−2.9	−4.9	−0.3	−4.6	−5.0
BR89c	0.9	−3.6	−4.5	1.7	−5.9	−7.6	−1.1	−7.7	−7.3

TABLE 3: Mean Absolute Error (kcal/mol) for the S_N2 Reactions (X = F, Cl, and Br)

xc functional	$\lvert\Delta E_{cmpx}\rvert$	$\lvert\Delta E_{ovr}\rvert$	$\lvert\Delta E_{centr}\rvert$
LDA	2.7	9.7	7.3
BLYP	1.1	6.7	7.5
BP	1.3	6.2	7.1
PW91	0.8	7.5	7.0
PBE	0.9	6.9	6.8
revPBE	1.5	4.6	6.0
OLYP	2.9	1.8	4.0
HCTH/93	3.0	1.9	3.9
HCTH/407	1.5	1.9	3.3
KCIS	1.7	2.4	4.3
PKZB	1.8	2.3	4.4
VS98	3.9	6.6	3.0
Bmτ1	1.7	4.0	4.8
BLAP3	1.7	3.7	4.6
OLAP3	3.1	2.7	1.1
B00c	1.4	2.7	4.2
BR89c	1.2	5.7	6.5

In turn, the combination OLAP3 yields the best central barriers, which are the key parameters for the kinetics of the S_N2 reaction. The corresponding average OLAP3 error of only 1.06 kcal/mol is definitely lower than the errors of other functionals (see Table 3). This improvement is due to both OPTX and the meta-GGA correlation functional LAP3. Indeed, change of the exchange functional from BLAP3 to OLAP3 reduces the average error by 3.56 kcal/mol (from 4.62 to 1.06 kcal/mol). The same change of exchange functional, but with LYP correlation, i.e., going from BLYP to OLYP, reduces the average error for central barriers by 3.55 kcal/mol (from 7.52 to 3.97 kcal/mol). The subsequent change of the correlation functional from OLYP to OLAP3 reduces the error further by 2.91 kcal/mol to 1.06 kcal/mol. For the overall barriers, the OLAP3 error of 2.74 kcal/mol is somewhat larger than the abovementioned smallest error of 1.81 kcal/mol of OLYP. However, OLAP3 is the only method in which, in agreement with the experiment, the overall barriers are present for X = Cl and Br, while in other methods they are absent, so that in the latter cases TSs are made artificially more stable than reagents (see Table 1). Somewhat larger OLAP3 errors for the overall barrier and the complexation energy in the case X = F are due to the apparent overestimation of the electron correlation in the F^- anion by LAP3.

Considering the successful performance of OLAP3 for the reaction barriers, it is interesting to note that neither OPTX nor LAP3 was parametrized especially for problematic systems. Indeed, the simple form of the OPTX functional,

$$E_{x\sigma}^{\mathrm{OPTX}} = -\int [1.05151 c_x + 1.43169 u_\sigma{}^2(\mathbf{r})] \rho_\sigma{}^{4/3}(\mathbf{r})\, d\mathbf{r} \quad (4.2)$$

$$u_\sigma(\mathbf{r}) = \frac{\gamma x_\sigma{}^2(\mathbf{r})}{1 + \gamma x_\sigma{}^2(\mathbf{r})} \quad (4.3)$$

where $x_\sigma = 2(6\pi^2)^{1/3} s_\sigma$, $c_x = (3/4)(6/\pi)^{1/3}$ is the Dirac coefficient, and $\gamma = 0.006$, has been chosen in ref 1 to reproduce the Hartree−Fock atomic exchange energies. In turn, the LAP3 functional contains the logarithmic and polynomial dependence on the argument $(t'_\sigma)^{1/2}\rho_\sigma{}^{1/3}$, where $t'_\sigma = \tau_\sigma^{\mathrm{LSDA}}/\tau'_\sigma$ and τ'_σ is the alternative to (1.4), the Laplacian-dependent form of the kinetic energy density:

$$t'_\sigma(\mathbf{r}) = -\frac{1}{2}\sum_i^{N_\sigma} \phi_{i\sigma}^*(\mathbf{r}) \nabla^2 \phi_{i\sigma}(\mathbf{r}) \quad (4.4)$$

The dependence on $(t'_\sigma)^{1/2}\rho_\sigma{}^{1/3}$ has been parametrized in ref 2 to reproduce the energies of (dynamical) Coulomb correlation in atoms and molecules with normal covalent bonds. In this sense, the successful performance of OLAP3 for the S_N2 reactions seems to be accidental. However, with the analysis of the previous sections in mind, one can understand that the true reason for the success of OLAP3 is the effective $s_\sigma{}^4$ dependence of OPTX and the molecular correction of LAP3 from τ'_σ as it has been discussed in the previous section. These factors lead to the corrected lower stability of TSs and, as a result, to the improved description of the reaction barriers with OLAP3.

To conclude, the results of this section confirm the above-mentioned rule of ref 19, according to which, S_N2 reactions with the three-center four-electron bonds in their TSs were designated as truly problematic cases for standard GGAs. In agreement with the conclusions of ref 19, better description of S_N2 reactions has been shown to result from improvement of the GGA exchange functionals.

V. Assessment of GGAs and Meta-GGAs for Hydrogen Abstraction Reactions

The prototype hydrogen abstraction reactions considered in this paper are listed in Table 4. The reference data for the energies of reactions E and the barriers of the forward E_{for} and reverse E_{rev} reactions of the first 14 reactions in Table 4 have been taken from the database of reactions proposed in ref 55. The geometries of the reagents and products are obtained at the quadratic single and double configuration interaction (QCISD) level of ab initio theory.[55] The barrier of the last reaction (also calculated with QCISD) has been taken from ref 56. In parentheses, we also report, if available, the careful estimates for the energy barriers extracted from experimental data, proposed in ref 57. However, these energies include zero point energy corrections and further corrections (tunneling corrections to canonical transition state theory applied to the experimental data) and, therefore, are not directly comparable to our calculated energies and those from the database of ref 55. The differences of the order of a few kilocalories per mole between the two sets highlight the care that has to be taken to obtain appropriate reference data to assess, or to parametrize, approximate DFT methods.

TABLE 4: Reference Data for the Prototype Hydrogen Abstraction and Exchange Reactions (All Energies Are in kcal/mol)[a]

reaction	E_{for}	E_{rev}	E
$HCl + H \rightarrow Cl + H_2$	5.6	8.7	−3.1
$OH + H_2 \rightarrow H + H_2O$	5.7 (3.9)	22.0 (18.5)	−16.3 (−14.6)
$CH_3 + H_2 \rightarrow H + CH_4$	12.1 (10.8)	15.0 (10.9)	−2.9 (−0.1)
$OH + CH_4 \rightarrow CH_3 + H_2O$	6.7 (4.7)	20.2	−13.5
$H + H_2 \rightarrow H_2 + H$	9.6	9.6	0.0
$OH + NH_3 \rightarrow H_2O + NH_2$	3.2 (1.4)	13.2	−10.0
$HCl + CH_3 \rightarrow Cl + CH_4$	1.8	7.8	−6.0
$F + H_2 \rightarrow H + HF$	1.8	33.2	−31.4
$OH + CH_3 \rightarrow O + CH_4$	7.8	13.7	−5.9
$H + PH_3 \rightarrow PH_2 + H_2$	3.2	25.5	−22.3
$H + ClH' \rightarrow HCl + H'$	18.0	18.0	0.0
$OH + H \rightarrow H_2 + O$	10.1	13.1(8.8)	−3.0
$H + H_2S \rightarrow H_2 + HS$	3.6	17.4	−13.8
$O + HCl \rightarrow OH + Cl$	9.8	9.9	−0.1
$H_2O + OH \rightarrow OH + H_2O$	10.1(8.6)	10.1(8.6)	0.0

[a] All data are from ref 55, except the last entry from ref 56. The data in parentheses are from ref 57, if available.

TABLE 5: Calculated Values E_{barr} and Errors ΔE_{barr} (kcal/mol) with Respect to Reference Data (See Table 4) of the Barrier Height for the Reaction (5.1)

xc functional	E_{barr}	ΔE_{barr}	xc functional	E_{barr}	ΔE_{barr}
LDA	−2.9	−12.5	KCIS	5.1	−4.5
PW91	3.3	−6.3	PKZB	5.5	−4.3
BLYP	3.1	−6.5	VS98	5.6	−4.0
BP	0.9	−8.8	Bmτ1	7.5	−2.1
PBE	3.7	−5.9	BLAP3	7.2	−2.4
revPBE	4.9	−4.7	OLAP3	7.7	−1.9
OLYP	3.6	−6.0	B00c	4.4	−5.2
HCTH/93	7.1	−2.5	BR89c	6.2	−3.4
HCTH/407	7.4	−2.2			

All GGA and meta-GGA calculations have been performed with the ADF program.[40−42] The energies E, E_{for}, and E_{rev} have been calculated in the post-LDA manner in the TZ2P basis of STOs.

A pure assessment of GGAs and meta-GGAs for the three-center three-electron bond can be provided with the simplest symmetrical hydrogen abstraction reaction,

$$H + H_2 \rightarrow H_2 + H \quad (5.1)$$

The symmetrical TS H···H···H consists of just this bond. Table 5 presents the calculated values of the barrier height E_{barr} (the reference value is $E_{\mathrm{barr}} = 9.6$ kcal/mol) for the reaction (5.1) together with the corresponding errors ΔE_{barr}. At first glance, the pattern of the performance of various functionals is similar to that established for the S_N2 reactions in the previous section. Again, LDA overbinds the TS with the large error $\Delta E_{\mathrm{barr}} = -12.49$ kcal/mol, i.e., the TS is 2.89 kcal/mol more stable than the reactants. Standard GGAs substantially reduce this error, though the remaining GGA errors are close to their typical errors for the S_N2 reactions (compare Tables 3 and 5). Modified GGAs and meta-GGAs reduce further the barrier error.

However, there is a qualitative difference between these two types of reactions in the importance of the exchange and correlation functionals for the observed improvement of the calculated barriers. While for the S_N2 reactions the major improvement comes from modification of the exchange functionals, this is not the case for the reaction (5.1). For example, as was mentioned in the previous section, modification of the exchange functional BR89 to the functional B00 with the t_σ-dependent correction factor f_σ of (3.9) reduces significantly the errors of the combination B00c for the S_N2 reaction barriers compared to those of BR89c (see Table 3). On the contrary, in

TABLE 6: Calculated Values E_{for}, E_{rev}, E and Errors ΔE_{for}, ΔE_{rev}, ΔE (kcal/mol) with Respect to Reference Data (See Table 4) of the Barrier Height for the Reaction HCl + H → Cl + H_2

xc functional	E_{for}	ΔE_{for}	E_{rev}	ΔE_{rev}	E	ΔE
LDA	−3.1	*−8.7*	−10.7	*−19.4*	7.6	*10.7*
PW91	0.0	*−5.6*	−1.6	*−10.3*	1.6	*4.7*
BLYP	−2.3	*−7.9*	2.7	*−6.02*	−5.0	*−1.9*
BP	−2.8	*−8.4*	0.2	*−8.5*	−3.0	*0.1*
PBE	0.7	*−4.9*	−1.2	*−9.9*	1.9	*5.0*
revPBE	1.1	*−4.5*	2.5	*−6.2*	−1.4	*1.7*
OLYP	−0.1	*−5.7*	4.0	*−4.7*	−4.1	*−1.0*
HCTH/93	1.8	*−3.8*	5.1	*−3.6*	−3.3	*−0.2*
HCTH/407	2.3	*−3.3*	3.8	*−4.9*	−1.5	*1.6*
KCIS	2.5	*−3.1*	3.0	*−5.7*	−0.5	*2.6*
PKZB	0.0	*−5.6*	5.8	*−2.9*	−5.8	*−2.6*
VS98	4.2	*−1.4*	3.1	*−5.6*	1.1	*4.0*
Bmτ1	1.9	*−3.7*	7.1	*−1.6*	−5.2	*−2.1*
BLAP3	1.9	*−3.7*	6.6	*−2.1*	−4.7	*−1.6*
OLAP3	4.1	*−1.5*	7.9	*−0.8*	−3.8	*−0.7*
B00c	0.8	*−4.8*	4.2	*−4.5*	−3.4	*−0.3*
BR89c	0.8	*−4.8*	3.1	*−5.6*	−2.3	*0.8*

TABLE 7: Calculated Values E_{for}, E_{rev}, E and Errors ΔE_{for}, ΔE_{rev}, ΔE (kcal/mol) with Respect to Reference Data (See Table 4) of the Barrier Height for the Reaction OH + CH_3 → O + CH_4

xc functional	E_{for}	ΔE_{for}	E_{rev}	ΔE_{rev}	E	ΔE
LDA	−9.4	*−17.2*	−9.6	*−23.3*	0.2	*6.1*
PW91	−0.8	*−8.6*	−0.2	*−13.9*	−0.6	*5.3*
BLYP	1.8	*−6.0*	2.2	*−11.5*	−0.4	*5.5*
BP	0.6	*−7.2*	1.3	*−12.4*	−0.7	*5.2*
PBE	−0.7	*−8.5*	0.2	*−13.5*	−0.9	*5.0*
revPBE	2.4	*−5.4*	4.1	*−9.6*	−1.7	*4.2*
OLYP	3.0	*−4.8*	6.6	*−7.1*	−3.6	*2.3*
HCTH/93	2.7	*−5.1*	7.1	*−6.6*	−4.4	*1.5*
HCTH/407	1.8	*−6.0*	6.2	*−7.5*	−4.4	*1.5*
KCIS	3.3	*−4.5*	7.1	*−6.6*	−3.8	*2.1*
PKZB	4.4	*−3.4*	8.8	*−4.9*	−4.4	*1.5*
VS98	3.1	*−4.7*	7.9	*−5.8*	−4.8	*1.1*
Bmτ1	5.5	*−2.3*	6.4	*−7.3*	−0.9	*5.0*
BLAP3	5.2	*−2.6*	6.1	*−7.7*	−0.9	*5.0*
OLAP3	6.5	*−1.3*	10.4	*−3.3*	−3.9	*2.0*
B00	3.3	*−4.5*	7.5	*−6.2*	−4.2	*1.7*
BR89c	1.8	*−6.0*	6.0	*−7.8*	−4.2	*1.7*

the case of (5.1), the same correction actually leads to a larger error of B00c for E_{barr} compared to BR89c (see Table 5). Note, as another example, that a change of the exchange functional from BLYP to OLYP reduces ΔE_{barr} by only 0.5 kcal/mol. This correlates with the normal behavior, established in Sections II and III, of the GGA argument s_σ^2 and the meta-GGA factor f_σ for the TS of the hydrogen abstraction reaction.

Unlike the S_N2 reaction, the major improvement for reaction (5.1) comes from modification of the correlation functional. Indeed, independently of whether B88 or OPTX is employed in the xc combination, a change of the correlation functional from LYP to LAP3 reduces ΔE_{barr} by 4.1 kcal/mol for BLAP3 or OLAP3 compared to the corresponding combination BLYP or OLYP. In the latter case, this reduction produces the smallest error among all functionals $\Delta E_{barr} = -1.94$ kcal/mol for OLAP3 (see Table 5). A slightly larger (in absolute value) error of −2.13 kcal/mol is produced with the combination Bmτ1 with the correlation functional τ1, which, as was mentioned above, is a modified version of LAP3.

In Tables 6 and 7 the calculated reaction energy E and the barriers E_{for} and E_{rev} are presented with the corresponding errors for two unsymmetrical hydrogen abstraction reactions, and Table 8 presents the average errors of the functionals for all 15 reactions. In general, because of the more complex nature of the reactants, the pattern of improvement due to the exchange and correlation functionals is more complicated than for reaction (5.1), though the general trend is the same. Standard GGAs reduce the large LDA average absolute errors for barriers from ca. 18.5 to 8.5−10.5 kcal/mol, with revPBE producing somewhat smaller errors of 6.75 and 7.46 kcal/mol for E_{for} and E_{rev}, respectively (see Table 8). They also reduce the substantial LDA reaction energy error of 6.33 kcal/mol, in particular; the corresponding revPBE error is only 1.16 kcal/mol.

TABLE 8: Mean Absolute Error (kcal/mol) for the Prototype Hydrogen Abstraction Reactions

xc functional	$\lvert\Delta E_{for}\rvert$	$\lvert\Delta E_{rev}\rvert$	$\lvert\Delta E\rvert$
LDA	18.6	18.5	6.3
PW91	9.9	10.5	2.7
BLYP	8.5	8.7	1.9
BP	9.9	10.3	1.6
PBE	9.5	10.2	2.7
RevPBE	6.8	7.5	1.2
OLYP	6.4	6.5	1.4
HCTH/93	5.1	5.1	1.1
HCTH/407	5.7	5.6	1.1
KCIS	5.4	6.6	1.3
PKZB	4.4	6.2	3.4
VS98	4.6	5.2	1.6
Bmτ1	4.2	4.6	1.9
BLAP3	4.5	4.8	1.7
OLAP3	2.7	3.5	1.6
B00c	5.3	5.8	1.2
BR89c	6.6	6.6	0.9

Further significant improvement of the calculated barriers is achieved with the use of the correlation functionals LAP3 and τ1. Indeed, a change of the exchange functional only, from B88 to OPTX, reduces ΔE_{for}^{av} by 2.1 kcal/mol from 8.5 kcal/mol for BLYP to 6.4 kcal/mol for OLYP, which is actually close to the abovementioned value of 6.75 kcal/mol for revPBE. On the other hand, a subsequent change of the correlation functional from LYP to LAP3, i.e., going from OLYP to OLAP3, produces further error reduction by 3.73 kcal/mol and the resultant smallest error among all functionals, $\Delta E_{for}^{av} = 2.67$ kcal/mol of OLAP3 (see Table 8). The combination OLAP3 also produces the best reverse barriers, with the average error $\Delta E_{rev}^{av} = 3.48$ kcal/mol. The second best barriers are produced with Bmτ1, with the average errors $\Delta E_{for}^{av} = 4.18$ kcal/mol and $\Delta E_{rev}^{av} = 4.64$ kcal/mol. Note that OLAP3 yields also reasonable reaction energies with an average error of 1.6 kcal/mol.

Finally, we present in Table 9 the barriers E_{barr} calculated for a particular case, the chemically important prototype reaction (1.5) of hydrogen abstraction from the water molecule: $H_2O + OH^\bullet \rightarrow OH^\bullet + H_2O$. They are compared with the accurate calculated QCISD(T) value of 10.1 kcal/mol;[56] the corresponding errors ΔE_{barr} are given in the third column of Table 9. In fact, just these errors have been taken to calculate the contribution of this reaction to the overall accuracy of the functionals in Table 8. All the methods hugely underestimate the barrier compared to the QCISD(T) reference and, though OLAP3 yields the least absolute error $\lvert \Delta E_{barr} \rvert = 6.41$ kcal/mol, it is considerably larger than the average errors presented in Table 8. However, the experimental estimate of the barrier, the Arrhenius activation energy of 4.2 kcal/mol,[58] is also substantially lower than the theoretical reference value. In this particular case, as was established in ref 56, the reason for the observed large discrepancy of the conventional quantum chemistry potential energy barrier and the experimental activation energy is the effective decrease of the activation energy compared to the potential energy due to the H atom tunneling. The deviations ΔE_{barr}^{exp} of the calculated barriers from the experiment are given

TABLE 9: Calculated Values E_{barr} (kcal/mol) for Various Functionals and the Differences ΔE_{barr} with Respect to the Theoretical QCISD(T) Reference Data (See Table 4) and ΔE_{barr}^{exp} with Respect to the Experimental Arrhenius Activation Energy at 300 K (See Text) of the Barrier Height for the Reaction $H_2O + OH^{\bullet} \rightarrow OH^{\bullet} + H_2O$

xc functional	E_{barr}	ΔE_{barr}	ΔE_{barr}^{exp}
LDA	−18.9	*−29.0*	*−23.1*
PW91	−7.5	*−17.6*	*−11.7*
BLYP	−4.3	*−14.4*	*−8.5*
BP	−5.8	*−15.9*	*−10.0*
PBE	−7.0	*−17.1*	*−11.2*
revPBE	−2.7	*−12.8*	*−6.9*
OLYP	−0.9	*−11.0*	*−5.1*
HCTH/93	−0.6	*−10.7*	*−4.8*
HCTH/407	−1.7	*−11.8*	*−5.9*
KCIS	−0.7	*−10.8*	*−4.9*
PKZB	1.1	*−9.0*	*−3.1*
VS98	0.9	*−9.2*	*−3.3*
Bmτ1	0.7	*−9.4*	*−3.5*
BLAP3	0.3	*−9.8*	*−3.9*
OLAP3	3.7	*−6.4*	*−0.5*
B00c	1.0	*−9.1*	*−3.2*
BR89c	−2.4	*−12.5*	*−6.6*

in the last column of Table 9. It is to be noted that the calculated OLAP3 value of 3.69 kcal/mol is very close to the abovementioned experimental value, so that the corresponding deviation is only −0.51 kcal/mol. Other functionals display considerably larger (in absolute value) deviations (see Table 9). One could exploit this curious property of the OLAP3 functional in MD calculations, where the atomic motions are treated classically, which is generally the case, even in Car−Parrinello-type MD calculations. (In general, of course, we do not wish to advocate treating nuclear motion classically on an erroneous potential surface to approximate quantum molecular dynamics using an accurate potential.)

In conclusion, just as in the case of the S_N2 reactions considered in the previous section, the original combination OLAP3 also shows the best overall performance for the hydrogen abstraction reactions. However, unlike the S_N2 reactions, the major improvement in the latter case is achieved with a change of the correlation functionals. This is in agreement with the analysis of ref 3, according to which the improvement in this particular normal case could be gained with the modification of the local spin density dependence of standard GGA correlation functionals. Apparently, such a modification has been effectively undertaken in ref 2, where the correlation energy functional LAP3 was constructed, explicitly taking into account the Coulomb correlation of the opposite- and like-spin electrons.

VI. Conclusions

The goal of this paper has been three-fold. First, to assess the quality of GGA and meta-GGA exchange and correlation functionals for the prototype S_N2 and hydrogen abstraction reactions. Second, to establish the specific topological features of the electron density of problematic (for standard GGAs) systems and to relate them to the orbital structure of the chemical bonds involved. Third, to try new xc combinations such as OLAP3 for the reactions.

A characteristic topological feature of the density of problematic systems has been established, which is the enhanced values of the basic gradient argument s_σ^2 with local maxima in the bonding region. With the direct evaluation of s_σ^2 for the simple $[He-He]^+$ bond, the origin of this topological feature has been traced to the occupation in problematic systems of valence orbitals with an antibonding or essentially nonbonding character. Such an electronic structure means that left−right correlation is not so strong as in a normal two-center two-electron bond. However, the localized nature of the effective exchange−correlation hole of the GGAs, which is correct for normal chemical bonds with significant nondynamical (left−right) correlation, persists in these problematic cases and causes the GGAs to yield a too negative energy. We have connected the special electronic structure of the problematic systems to a topological feature of the electron density that enters the functional forms of the GGAs and causes them to exhibit the too stabilizing behavior. This topological feature of the electron density is the local enhancement of s_σ^2 in the bonding region. The way that the standard GGAs depend on s_σ^2 leads them to overestimate the stability of problematic systems. We have demonstrated that the behavior of s_σ^2 is also reflected in special behavior of the topological features of the density that are being used in meta-GGAs, such as the ratio $t_\sigma(\mathbf{r})$ (cf. eq 3.1) between the LDA kinetic energy density $\tau_\sigma^{LDA}(\mathbf{r})$ and the Kohn−Sham kinetic energy density $\tau_\sigma^{s}(\mathbf{r})$ and the related correction factor f_σ. This provides some understanding of why modified GGA functionals that have a special dependence on s_σ^2, such as the functionals OPTX and HCTH with a leading s_σ^4 behavior of the gradient corrections, or the meta-GGAs with $t_\sigma(\mathbf{r})$ dependence, can improve on the standard GGAs for the problematic cases.

The performance of 17 GGA and meta-GGA functionals has been assessed for the prototype problematic cases, the symmetrical S_N2 reactions. Standard GGAs already reduce substantially the reaction barriers calculated by LDA, but they still have barriers that are too low. Important further error reduction is gained with the modified GGAs and meta-GGAs. The best overall performance has been observed for the combination OLAP3. The basis of this success is the dependence of the exchange OPTX functional with the effective leading s_σ^4 term of its gradient correction. Another factor appears to be the dependence of the correlation LAP3 functional on the meta-GGA argument.

The performance of GGA and meta-GGA functionals has also been assessed for 15 hydrogen abstraction reactions. These transition states have not been categorized as problematic in the same way as the transition state of the S_N2 reactions, since the hydrogen abstraction transition states have considerable nondynamical correlation, which is in keeping with the localized exchange−correlation hole of the GGAs. However, the GGA correlation functionals in this case overestimate the dynamical correlation, which presumably could be remedied by exploiting the local spin polarization $\zeta(\mathbf{r})$.[19] We find, indeed, for the present series of hydrogen abstraction reactions that standard GGAs, even though they reduce substantially the large error in the reaction barriers calculated by LDA, still yield significant errors. However, further reduction is obtained, mainly due to the modified correlation functionals. Again, the best overall performance has been observed for OLAP3. For the considered systems with nonzero spin-density the basis of the success of OLAP3 appears to be the modified structure of the correlation functional LAP3, which takes explicitly into account the Coulomb correlation of the opposite- and like-spin electrons.

The analysis of the behavior of s_σ^2 and the meta-GGA correction factor f_σ confirms the qualitative rule of ref 19. Indeed, for the system H + ClH, with the three-center three-electron ($n/m = 1$) bond, s_σ^2 and f_σ behave like the case of the molecule N_2. On the other hand, for the problematic system $[F\cdots CH_3\cdots F]^-$ with the three-center four-electron ($n/m = 4/3$)

bond, s_σ^2 and f_σ behave like for the prototype problematic system He_2^+ with the two-center three-electron ($n/m = 3/2$) bond. The results of the GGA and meta-GGA calculations also confirm the conclusions of ref 19, in the sense that for the problematic case of the S_N2 reactions, the improvement of the results has been achieved with the modified exchange energy functionals, while for the normal case of the hydrogen abstraction reactions the improvement has been achieved with the modified correlation energy functionals.

On the basis of the assessment performed in this paper, we can recommend the combination OLAP3 for calculations of chemical reactions. For the considered prototype reactions, OLAP3 produces the best overall reaction barriers, and it also reproduces well the energies of the hydrogen abstraction reactions. On the other hand, OLAP3 is certainly not the best functional for thermochemical calculations. Our calculations for the standard thermochemical G2 set of molecules show that the quality of OLAP3 for these calculations is superior to that of BP, but it is somewhat inferior to that of BLYP, and it is definitely worse than the quality of the meta-GGA functional VS98. With this, OLAP3 can only be considered as yet another approach to the universally good xc functional. The challenge is to develop a functional which would then combine the quality of OLAP3 for chemical reactions and that of VS98 for thermochemistry. We hope that the analysis and the assessment performed in this paper can serve this goal.

References and Notes

(1) Handy, N. C.; Cohen, A. J. *Mol. Phys.* **2001**, *99*, 403.
(2) Proynov, E. I.; Sirois, S.; Salahub, D. R. *Int. J. Quantum Chem.* **1997**, *64*, 427.
(3) Schipper, P. R. T.; Gritsenko, O. V.; Baerends, E. J. *J. Chem. Phys.* **1999**, *111*, 4056.
(4) Bally, T.; Sastry, G. N. *J. Phys. Chem. A* **1997**, *101*, 7923.
(5) Braida, B.; Hiberty, P. C.; Savin, A. *J. Phys. Chem. A* **1998**, *102*, 7872.
(6) Sodupe, M.; Bertran, J.; Rodriguez-Santiago, L.; Baerends, E. J. *J. Phys. Chem. A* **1999**, *103*, 166.
(7) Johnson, B. G.; Gonzales, C. A.; Gill, P. M. W.; Pople, J. A. *Chem. Phys. Lett.* **1994**, *221*, 100.
(8) Baker, J.; Muir, M.; Andzelm, J. *J. Chem. Phys.* **1995**, *102*, 2063.
(9) Porezag, D.; Pederson, M. R. *J. Chem. Phys.* **1995**, *102*, 9345.
(10) Jursic, B. S. *Theor. Comput. Chem.* **1996**, *4*, 709.
(11) Skokov, S.; Wheeler, R. A. *Chem. Phys. Lett.* **1997**, *271*, 251.
(12) Chermette, H.; Razafinjanahary, H.; Carrion, L. *J. Chem. Phys.* **1997**, *107*, 10643.
(13) Csonka, G. I.; Johnson, B. G. *Theor. Chem. Acc.* **1998**, *99*, 158.
(14) Filatov, M.; Thiel, W. *Chem. Phys. Lett.* **1998**, *295*, 467.
(15) Deng, L.; Branchadell, V.; Ziegler, T. *J. Am. Chem. Soc.* **1994**, *116*, 10645.
(16) Glukhovtsev, M. N.; Bach, R. D.; Pross, A.; Radom, L. *Chem. Phys. Lett.* **1996**, *260*, 558.
(17) Streitwieser, A.; Choy, G. S.-C.; Abu-Hasanayn, F. *J. Am. Chem. Soc.* **1997**, *119*, 5013.
(18) Grüning, M.; Gritsenko, O. V.; van Gisbergen, S. J. A.; Baerends, E. J. *J. Phys. Chem. A* **2001**, *105*, 9211.
(19) Gritsenko, O. V.; Ensing, B.; Schipper, P. R. T.; Baerends, E. J. *J. Phys. Chem. A* **2000**, *104*, 8558.
(20) Perdew, J. P. *Phys. Rev. B* **1986**, *33*, 8822 (Erratum: *Phys. Rev. B* **1986,** *34*, 7406).
(21) Perdew, J. P.; Burke, K.; Wang, Y. *Phys. Rev. B: Condens. Matter Mater. Phys.* **1996**, *54*, 16533.
(22) Lee, C.; Yang, W.; Parr, R. G. *Phys. Rev. B: Condens. Matter Mater. Phys.* **1988**, *37*, 785.
(23) Becke, A. *Phys. Rev. A: At., Mol., Opt. Phys.* **1988**, *38*, 3098.
(24) Herman, F.; van Dyke, J. P.; Ortenburger, I. B. *Phys. Rev. Lett.* **1969**, *22*, 807.
(25) Perdew, J. P. Unified Theory of Exchange and Correlation beyond the Local Density Approximation. In *Electronic Structure of Solids*; Ziesche, P., Eschrig, H., Eds.; Akademie Verlag: Berlin, 1991; p 11.
(26) Perdew, J. P.; Chevary, J. A.; Vosko, S. H.; Jackson, K. A.; Pederson, M. R.; Singh, D. J.; Fiolhais, C. *Phys. Rev. B: Condens. Matter Mater. Phys.* **1992**, *46*, 6671.
(27) Perdew, J. P.; Burke, K.; Ernzerhof, M. *Phys. Rev. Lett.* **1996**, *77*, 3865.
(28) van Leeuwen, R.; Baerends, E. J. *Int. J. Quantum Chem.* **1994**, *52*, 711.
(29) Cook, M.; Karplus, M. *J. Phys. Chem.* **1987**, *91*, 31.
(30) Gritsenko, O. V.; Schipper, P. R. T.; Baerends, E. J. *J. Chem. Phys.* **1997**, *107*, 5007.
(31) Hamprecht, F. A.; Cohen, A. J.; Tozer, D. J.; Handy, N. C. *J. Chem. Phys.* **1998**, *109*, 6264.
(32) Becke, A. D. *J. Chem. Phys.* **2000**, *112*, 4020.
(33) Becke, A. D.; Roussel, M. R. *Phys. Rev. A: At., Mol, Opt. Phys.* **1989**, *39*, 3761.
(34) Becke, A. D. *J. Chem. Phys.* **1988**, *88*, 1053.
(35) Becke, A. D. *Int. J. Quantum Chem., Quantum Chem. Symp.* **1994**, *28*, 625.
(36) van Voorhis, T.; Scuseria, G. E. *J. Chem. Phys.* **1998**, *109*, 400.
(37) Perdew, J. P.; Kurth, S.; Zupan, A.; Blaha, P. *Phys. Rev. Lett.* **1999**, *82*, 2544.
(38) Krieger, J. B.; Chen, J.; Iafrate, G. J.; Savin, A. In *Electron Correlations and Materials Properties*; Gonis, A., Kioussis, N., Eds.; Plenum Press: New York, 1999.
(39) Proynov, E. I.; Chermette, H.; Salahub, D. R. *J. Chem. Phys.* **2000**.
(40) Fonseca Guerra, C.; Snijders, J. G.; te Velde, G.; Baerends, E. J. *Theor. Chem. Acc.* **1998**, *99*, 391.
(41) te Velde, G.; Bickelhaupt, F. M.; van Gisbergen, S. J. A.; Fonseca Guerra, C.; Baerends, E. J.; Snijders, J. G.; Ziegler, T. *J. Comput. Chem.* **2001**, *22*, 931.
(42) Baerends, E. J.; Autschbach, J. A.; Bérces, A.; Bo, C.; Boerrigter, P. M.; Cavallo, L.; Chong, D. P.; Deng, L.; Dickson, M.; Ellis, D. E.; Fan, L.; Fischer, T. H.; Fonseca Guerra, C.; van Gisbergen, S. J. A.; Groeneveld, J. A.; Gritsenko, O. V.; Grüning, M.; Harris, F. E.; van den Hoek, P.; Jacobsen, H.; van Kessel, G.; Kootstra, F.; van Lenthe, E.; Osinga, V. P.; Patchkovskii, S.; Philipsen, P. H. T.; Post, D.; Pye, C. C.; Ravenek, W.; Ros, P.; Schipper, P. R. T.; Schreckenbach, G.; Snijders, J. G.; Sola, M.; Swart, M.; Swerhone, D.; te Velde, G.; Vernooijs, P.; Versluis, L.; Visser, O.; van Wezenbeek, E.; Wiesenekker, G.; Wolff, S. K.; Woo, T. K.; Ziegler, T. *ADF2002.02 (development/modified) 2002, SCM, Theoretical Chemistry*; Vrije Universiteit: Amsterdam; 2002.
(43) Glukhovtsev, M. N.; Pross, A.; Radom, L. *J. Am. Chem. Soc.* **1995**, *117*, 2024.
(44) Wladkowski, B. D.; Allen, W. D.; Brauman, J. I. *J. Phys. Chem.* **1994**, *98*, 13532.
(45) Barlow, S. E.; van Doren, J. M.; Bierbaum, V. M. *J. Am. Chem. Soc.* **1988**, *110*, 7240.
(46) Larson, J. W.; McMahon, T. B. *J. Am. Chem. Soc.* **1985**, *107*, 766.
(47) Dougherty, R. C.; Dalton, J.; Roberts, J. D. *Org. Mass Spectrom.* **1974**, *8*, 77.
(48) Wilbur, J. L.; Wladkowski, B. D.; Brauman, J. I. *J. Am. Chem. Soc.* **1993**, *115*, 10823.
(49) Pellerite, M. J.; Brauman, J. I. *J. Am. Chem. Soc.* **1983**, *105*, 2672.
(50) Tucker, S. C.; Truhlar, D. G. *J. Am. Chem. Soc.* **1990**, *112*, 3338.
(51) Wladkowski, B. D.; Brauman, J. I. *J. Phys. Chem.* **1993**, *97*, 13158.
(52) Jarecki, A. A.; Davidson, E. R. *Chem. Phys. Lett.* **1998**, *300*, 44.
(53) Gonzales, J. M.; Cox, S. R., III; Brown, S. T.; Allen, W. D.; Schaefer, H. F., III. *J. Phys. Chem. A* **2001**, *105*, 11327.
(54) Patchkovskii, S.; Ziegler, T. *J. Chem. Phys.* **2002**, *116*, 7806.
(55) Lynch, B. J.; Truhlar, D. G. *J. Phys. Chem. A* **2002**, *106*, 842.
(56) Hand, M. R.; Rodriquez, C. F.; Williams, I. H.; Balint-Kurti, G. G. *J. Phys. Chem. A* **1998**, *102*, 5958.
(57) Kang, J. K.; Musgrave, C. B. *J. Chem. Phys.* **2001**, *115*, 11040.
(58) Dubey, M. K.; Mohrschladt, R.; Donahue, N. M.; Anderson, J. G. *J. Phys. Chem. A* **1997**, *101*, 1494.